PHYSICS

Quantum localization bounds Trotter errors in digital quantum simulation

Markus Heyl[1]*, Philipp Hauke[2,3], Peter Zoller[4,5]

A fundamental challenge in digital quantum simulation (DQS) is the control of an inherent error, which appears when discretizing the time evolution of a quantum many-body system as a sequence of quantum gates, called Trotterization. Here, we show that quantum localization-by constraining the time evolution through quantum interference-strongly bounds these errors for local observables, leading to an error independent of system size and simulation time. DQS is thus intrinsically much more robust than suggested by known error bounds on the global many-body wave function. This robustness is characterized by a sharp threshold as a function of the Trotter step size, which separates a localized region with controllable Trotter errors from a quantum chaotic regime. Our findings show that DQS with comparatively large Trotter steps can retain controlled errors for local observables. It is thus possible to reduce the number of gate operations required to represent the desired time evolution faithfully.

INTRODUCTION

Quantum computers promise to solve certain computational problems exponentially faster than any classical machine (*1*). A particularly promising application is the solution of quantum many-body problems (*2*), with large potential impact on quantum chemistry, material science, and fundamental physics. The devices used in this effort can be divided into two major classes: analog quantum simulators, where the Hamiltonian of interest is engineered to mimic the desired quantum many-body physics; and digital quantum simulators (DQSs), where a target time-evolution operator is represented by a sequence of elementary quantum gates. The digital approach is particularly flexible since a universal digital quantum simulator can be freely programmed to simulate the unitary evolution of any many-body Hamiltonian with local interactions (Fig. 1A) (*3*). Recent experiments have demonstrated remarkable progress in implementing digital quantum simulation (DQS), e.g., by simulating simple molecules in quantum chemistry (*4*–*6*), condensed-matter models (*7*–*12*), and lattice gauge theories (*13*).

The working principle of DQS is as follows. Suppose that the target Hamiltonian $H = \sum_{l=1}^{M} H_l$ can be decomposed into M terms whose time evolution operators $U_l(t) = \exp(-itH_l)$ can be implemented on the considered quantum computing device. Using the Suzuki-Trotter formula, the full time-evolution operator $U(t) = \exp(-itH)$ can be approximated by discretizing it into $n \in N$ repetitions of the fundamental gates U_i

$$U^{(n)}(t) = \left[U_1\left(\frac{t}{n}\right)U_2\left(\frac{t}{n}\right)\ldots U_M\left(\frac{t}{n}\right)\right]^n \quad (1)$$

This Trotterization comes inherently with an error that can be rigorously upper bounded via the accuracy of the global unitary time-evolution operator (*3*)

$$U(t) - U^{(n)}(t) = \frac{t^2}{n}\sum_{l>m=1}^{M}[H_l, H_m] + \epsilon \quad (2)$$

Here, ϵ subsumes terms of order t^3/n^2 and higher. According to Eq. 2, for the lowest-order corrections, the Trotter error on the full time-evolution operator may grow quadratically with total simulation time t and (in generic quantum many-body systems) linearly in the number of simulated degrees of freedom N. It is possible to improve this upper bound, but an error bound that scales less than linear in t is not possible if one is concerned with the entire unitary operator (*14*). Although the polynomial scaling with both t and N is efficient in a computational complexity sense, it poses a substantial challenge for practical computations (*15*, *16*), seemingly preventing current technology from simulating all but small instances. As we show in this article, these generic bounds on the global many-body wave function overestimate by far the actual error on local observables such as magnetizations or low-order correlation functions. For example, in the DQS of a quantum Ising chain, the deviation of the magnetization dynamics from the ideal evolution can be considerably smaller and remain bounded even at long times (see Fig. 1B). It is the purpose of this article to explain this observation from physical grounds and thus assign a physical interpretation to Trotter errors.

We achieve this by linking Trotter errors to quantum localization. Localization is a ubiquitous phenomenon with many facets. Initially, it has been introduced to understand the absence of transport in systems of free particles with disorder (*17*). Since then, the concept has been generalized to various contexts such as many-body localization in Hilbert space as absence of quantum ergodicity (*18*) or energy localization in periodic time-dependent quantum many-body systems as absence of heating in continuously driven systems (*19*). As we show here, there occurs a related localization in Hilbert space at small Trotter steps that bounds time-discretization errors on local observables occurs. Our aim is to isolate the role of this universal error source, for which we focus in the following mostly on an idealized setting. We discuss the interplay of the Trotter errors with other, platform-dependent error sources in the concluding remarks and in the Supplementary Materials.

RESULTS

Trotter sequences as Floquet systems

In this work, we interpret the Trotterized evolution as a periodically time-dependent quantum many-body system with a period $\tau = t/n$ (see Fig. 1). The desired stroboscopic dynamics is therefore governed

[1]Max Planck Institute for the Physics of Complex Systems, Nöthnitzer Str. 38, 01187 Dresden, Germany. [2]Kirchhoff-Institute for Physics, Heidelberg University, 69120 Heidelberg, Germany. [3]Institute for Theoretical Physics, Heidelberg University, 69120 Heidelberg, Germany. [4]Institute for Quantum Optics and Quantum Information of the Austrian Academy of Sciences, 6020 Innsbruck, Austria. [5]Institute for Theoretical Physics, University of Innsbruck, 6020 Innsbruck, Austria.
*Corresponding author. Email: heyl@pks.mpg.de

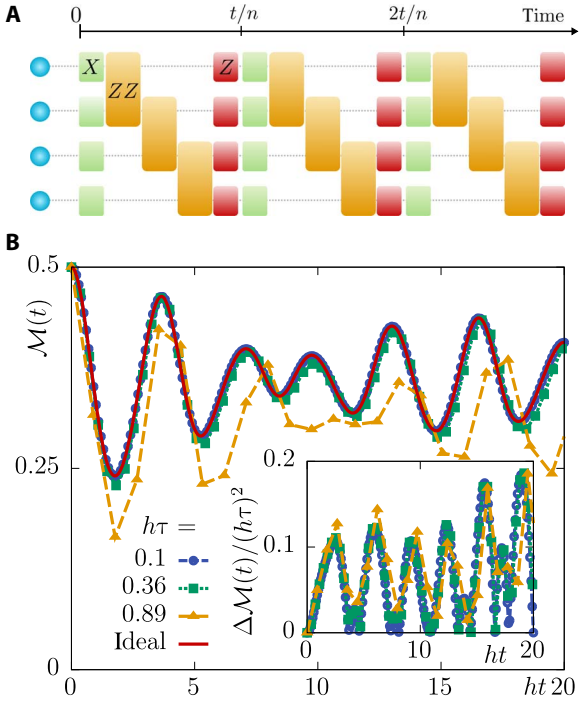

Fig. 1. Trotterized time evolution and resulting error on local observables. (**A**) Gate sequence for the digital quantum simulation (DQS) of an Ising model. The desired evolution up to total simulation time t is split into n repeated sequences of length $\tau = t/n$, each decomposed into fundamental quantum gates. The example shows a gate sequence for a four-qubit chain with Ising spin-spin interactions (ZZ) and transverse and longitudinal fields (simulated by single-qubit operations along the X and Z directions on the Bloch sphere). (**B**) Magnetization dynamics $\mathcal{M}(t) = N^{-1}\Sigma_{l=1}^{N}\langle S_l^z(t)\rangle$ in the DQS of the Ising model for $N = 20$ spins and different Trotter step sizes τ compared to the exact solution. The normalized deviation $\Delta\mathcal{M}(t)/(h\tau)^2$ with $\Delta\mathcal{M}(t) = |\mathcal{M}_{\tau=0}(t) - \mathcal{M}(t)|$ from the ideal dynamics shows a collapse of the error dynamics $\mathcal{M}_{\tau=0}(t)$ for sufficiently small τ.

by an associated Floquet Hamiltonian H_F, which we define for later convenience in the following form

$$e^{-iH_F\tau} = U_1(\tau)U_2(\tau)\ldots U_M(\tau) \tag{3}$$

The starting point of our considerations is an analytical expression for H_F in the limit of sufficiently small Trotter steps τ

$$H_F = H + i\frac{\tau}{2}\sum_{l>m}[H_l, H_m] + \mathcal{O}(\tau^2) \tag{4}$$

This form, which can be obtained from Eq. 3 via a Magnus expansion, quantifies the Trotterization error on a Hamiltonian level. There remain, however, two fundamental questions that we aim to address in this work: (i) What is the radius of convergence τ^* of this expansion? [Mathematically rigorous bounds for the convergence radius of the Magnus expansion do exist, but their applicability to generic quantum many-body systems is not often evident (*19*, *20*).] (ii) What is the influence of corrections to H that appear in H_F on the long-time dynamics of local observables? Recent theoretical predictions for heating in generic quantum many-body systems subject to a periodic drive might leave a rather pessimistic impression (*21*–*23*). We show in this work that the errors on local observables can nevertheless be controlled for all practical purposes. Throughout this work, we adopt the notion of local observables to be operators that include a bounded number of constituents. This definition includes local order parameters and typical correlation functions. These are not only generically the measures to describe the properties of physical systems, they are also the quantities that can be experimentally measured in a scalable way. Moreover, our general argumentation holds for physical Hamiltonians with few-body interactions, which for almost all of our discussion may even be taken to be long-ranged, except if otherwise stated.

Benchmark model: Quantum Ising chain

In the following, we illustrate our discussion with a generic, experimentally relevant model, the quantum Ising chain with Hamiltonian $H = H_Z + H_X$, with $H_Z = J\Sigma_{l=1}^{N-1}S_l^zS_{l+1}^z + h\Sigma_{l=1}^{N}S_l^z$ and $H_X = g\Sigma_{l=1}^{N}S_l^x$. Here, S_l^γ ($\gamma = x, y, z$) denotes spin-$^1/_2$ operators at lattice sites $l = 1,\ldots, N$. These models are paradigmatic workhorses for DQS platforms such as nuclear magnetic resonance (*24*), trapped ions (*7*), and superconducting qubits (*25*). As an initial state, we choose $|\psi_0\rangle = \otimes_l|\uparrow\rangle_l$, which can be prepared with high fidelity (*7*, *25*, *26*). In the remainder, we use the parameters $h/J = g/J = 1$ and choose to measure times in the characteristic scale h^{-1}. For details about the simulations including the used gate sequences, see Materials and Methods. Although we focus on this model, our findings also apply to other systems and thus seem generic (see also the Supplementary Materials where we provide a similar analysis for the lattice Schwinger model).

Quantum many-body chaos threshold

As the central result of this work, we connect Trotter errors in DQS with a threshold separating a many-body quantum chaotic region from a localized regime, thus linking the intrinsic accuracy of DQS with a quantum many-body phenomenon. For that purpose, we first investigate the inverse participation ratio (IPR)

$$\mathrm{IPR} = \sum_\nu p_\nu^2,\ p_\nu = |\langle\phi_\nu|\psi_0\rangle|^2 \tag{5}$$

with $|\phi_\nu\rangle$ denoting a full set of eigenstates of the Floquet Hamiltonian H_F. The IPR measures the localization properties of the state $|\psi_0\rangle$ in the eigenbasis $|\phi_\nu\rangle$, which is well studied also in the single-particle context (*27*). In a quantum chaotic delocalized regime, $|\psi_0\rangle$ is scrambled across the full eigenbasis implying a uniform distribution $p_\nu \to \mathcal{D}^{-1}$, with $\mathcal{D}$ as the number of available states in Hilbert space. Since $\mathcal{D}$ grows exponentially with the number of degrees of freedom N, we introduce the rate function $\lambda_\mathcal{D} = N^{-1}\log(\mathcal{D})$, which exhibits a well-defined thermodynamic limit. Analogously, we define $\lambda_{\mathrm{IPR}} = -N^{-1}\log(\mathrm{IPR})$. In Fig. 2A, we show numerical data for the ratio $\lambda_{\mathrm{IPR}}/\lambda_\mathcal{D}$ for the considered benchmark example. For the data in this plot, we take into account the expected leading-order finite-size corrections $\lambda_\mathcal{D} = N^{-1}[\log(\mathcal{D}) - \log(2)]$ in the delocalized regime, which can be estimated using random matrix theory (*28*). As one can see, there appears a sharp threshold separating a quantum chaotic regime at large Trotter steps, where λ_{IPR} tends to $\lambda_\mathcal{D}$ with increasing system size, from a regular region with $\lambda_{\mathrm{IPR}}/\lambda_\mathcal{D} < 1$.

A strong fingerprint of quantum chaos can also be found in out-of-time–ordered (OTO) correlators, which quantify how fast

quantum information scrambles through a many-body system. A typical OTO correlator is of the form

$$\mathcal{F}(t) = \langle V^\dagger(t) W^\dagger V(t) W \rangle \tag{6}$$

where $V(t)$ denotes the time evolution of the operator V in the Heisenberg picture. While quantum chaos via OTO correlators is conventionally diagnosed by considering a late-time exponential growth for operators V and W with finite support in real space (*29*), here, we consider the asymptotic long-time value of the extensive operator $V = W = N^{-1}\Sigma_l S_l^z$ (*30*). We estimate the corresponding long-time limit, $\mathcal{F} = \mathcal{F}(t \to \infty)$, via a stroboscopic average $\mathcal{F} = \lim_{n\to\infty} n^{-1}\Sigma_{l=1}^{n}\mathcal{F}(l\tau)$.

In Fig. 2B, we present numerical evidence that this quantity detects the many-body quantum chaos threshold that we have seen in the IPR. There is a clear threshold that separates a localized region at small Trotter steps τ, where $\mathcal{F} > 0$, from a quantum chaotic region at large τ, where $\mathcal{F} \to 0$. The vanishing OTO correlator in the many-body quantum chaotic regime can be understood directly from the results obtained for the IPR. Consider the spectral decomposition of a local Hermitian operator $V = \Sigma_\alpha \lambda_\alpha |\alpha\rangle\langle\alpha|$, with λ_α as the eigenvalues and $|\alpha\rangle$ as the eigenvectors of V (for the considered magnetization, these are equivalent to the set of spin configurations). The effective Floquet dynamics yields after n periods

$$V(n\tau) = \sum_{\alpha}\sum_{\nu,\mu} \lambda_\alpha C_{\nu\alpha} C^*_{\mu\alpha} e^{-i(E_\nu - E_\mu)n\tau} |\phi_\nu\rangle\langle\phi_\mu| \tag{7}$$

with the Floquet quasi-energy corresponding to the eigenstate $|\phi_\nu\rangle$ and $C_{\nu\alpha} = \langle\phi_\nu|\alpha\rangle$.The behavior of the IPR suggests that for all spin configurations, $p_{\nu\alpha} \equiv |C_{\nu\alpha}|^2 = \mathcal{D}^{-1}$ is uniformly distributed, such that the amplitudes $C_{\nu\alpha}$ are almost structureless and contain only a phase information, $C_{\nu\alpha} = \mathcal{D}^{-1/2} e^{i\varphi_{\nu\alpha}}$. After sufficiently many Floquet cycles, this phase information is randomized and scrambled by the unitary evolution, except when $\nu = \mu$, projecting the operator to the so-called diagonal ensemble (*31*). Thus, for $n \to \infty$, one obtains $V(n\tau) \to \mathcal{D}^{-1}\Sigma_\alpha \lambda_\alpha \mathbb{1}$. Here, $\mathcal{D}^{-1}\Sigma_\alpha \lambda_\alpha = \mathcal{D}^{-1}\mathrm{Tr}V$ is equivalent to the infinite-temperature average, which yields a vanishing value for the considered total magnetization. That is, the operator becomes completely scrambled over the full Hilbert space.

Within the localized phase, the amplitudes $C_{\nu\alpha}$ contain more structure than only the phase information, which yields a nonzero value for the OTO correlator. For small systems, such as for $N = 10$ in Fig. 2B, one can observe additional structures in the crossover region, which vanish for larger N. We attribute these to individual quantum many-body resonances, which can be resolved in small systems but which merge for large N.

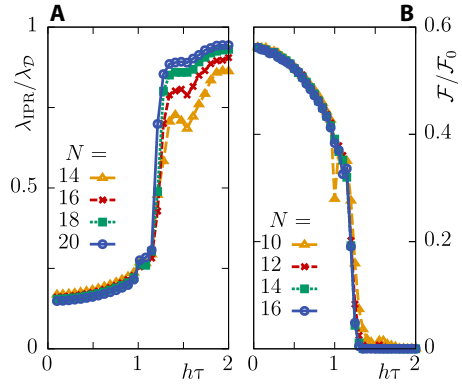

Fig. 2. Localization and quantum chaos in the Trotterized dynamics of the quantum Ising chain. (**A**) Rate function λ_{IPR} of the IPR, normalized to the maximally achievable value $\lambda_{\mathcal{D}}$ describing uniform delocalization over all accessible states. A sharp threshold as a function of the Trotter step size τ separates a localized regime at small τ from a quantum chaotic regime at large τ. (**B**) The long-time limit $\mathcal{F}$ of the OTO correlator also signals a sharp quantum chaos threshold. $\mathcal{F}$ is normalized with respect to $\mathcal{F}_0 = {}^1/_8$, the theoretical maximum. Full scrambling is only achieved for large Trotter steps.

Robustness of local observables

While the corrections due to time discretization are weak on a Hamiltonian level, as seen in the Magnus expansion in Eq. 4, there is a priori no guarantee that the long-time dynamics is equally well reproduced. It is, e.g., well known for classical chaotic systems that even weak perturbations can grow quickly in time. Here, we provide numerical evidence that in the localized regime, the dynamics of local observables remains constrained and controlled, even in the long-time limit. This asymptotic long-time dynamics is a worst-case scenario for DQS: When Trotter errors on local observables can be controlled in this limit, so can they on shorter times. In the Supplementary Materials, we also discuss the buildup of Trotter errors on short to intermediate times in more detail.

In Fig. 3A, we show the asymptotic long-time value $\mathcal{M}$ of the magnetization, $\hat{\mathcal{M}}(t) = N^{-1}\Sigma_l S_l^z(t)$. One can observe that the many-body quantum chaos threshold identified in the IPR and OTO correlator has a substantial influence on the long-time Trotter error of local observables such as $\mathcal{M}(t)$. For large Trotter steps τ, the magnetization

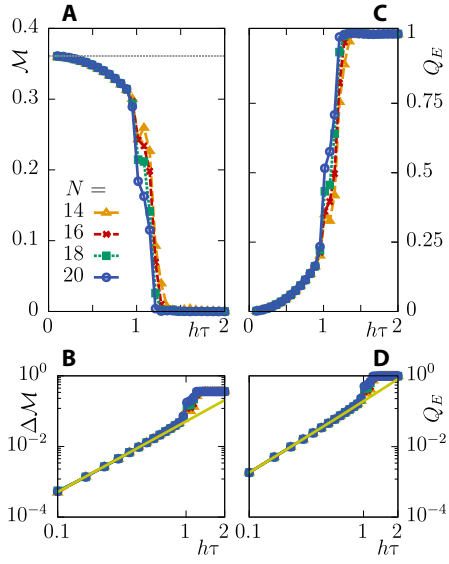

Fig. 3. Trotter errors for local observables in the infinite long-time limit for the Ising model. Both the magnetization $\mathcal{M}$ (**A**) and simulation accuracy Q_E (**C**) exhibit a sharp crossover from a regime of controllable Trotter errors for small Trotter steps τ to a regime of strong heating at larger τ. The dashed line in (A) refers to the desired case of the ideal evolution. The Trotter error exhibits a quadratic scaling at small τ for both the deviation of the magnetization, $\Delta\mathcal{M} = \mathcal{M} - \mathcal{M}_{\tau=0}$, (**B**) and Q_E (**D**). The solid lines in (B) and (D) represent analytical results obtained perturbatively in the limit of small Trotter steps τ. These results indicate the controlled robustness of digital quantum simulation against Trotter errors, in the long-time limit and largely independent of N.

acquires its infinite-temperature value, perfectly consistent with the above analysis of the fully delocalized quantum chaotic phase. However, for small Trotter steps, the error $\Delta\mathcal{M}$ relative to the targeted dynamics exhibits a quadratic dependence in τ, as we show in Fig. 3B. The origin of these weak Trotter errors can already be identified from the dynamical trajectories of the magnetization shown in the inset of Fig. 1B, where we plot the error $\Delta\mathcal{M}(t)$ for different Trotter steps normalized with respect to $(h\tau)^2$. We observe a collapse of trajectories corresponding to different τ, with the overall magnitude of the error remaining bounded in time. This finding suggests that in the localized phase, the discretization error on local observables itself shows regular behavior, in the sense that different perturbation strengths as measured by τ do not yield fast diverging expectation values.

Simulation accuracy

In the previous sections, we have provided evidence for a sharp threshold between a delocalized and a localized regime with controllable Trotter errors. We now aim to understand the influence of the regular regions onto the dynamics of local observables. We identify as the underlying reason for the weak Trotter errors a dynamical constraint due to an emergent stroboscopic constant of motion in the effective time-periodic problem, which is the Floquet Hamiltonian H_F. Although this integral of motion is different from the desired energy conservation of the target Hamiltonian H, the perturbative expansion in Eq. 4 suggests a close connection. It is therefore natural to quantify the accuracy of DQS by measuring how far the system deviates from the desired constant of motion H via

$$Q_E(n\tau) \equiv \frac{E_\tau(n\tau) - E_0}{E_{T=\infty} - E_0} \tag{8}$$

Here, we have introduced $E_\tau(n\tau) = \langle H(n\tau)\rangle_\tau$ and $E_0 = E_{\tau\to 0}(n\tau) = \langle\psi_0|H|\psi_0\rangle$, where the subindex τ refers to the used Trotter step for the dynamics. In $Q_E(t)$, we normalize the errors using the system's energy at infinite temperature, $E_{T=\infty} = \mathcal{D}^{-1}\mathrm{Tr}H$. In the idealized limit $\tau \to 0$, where the integral of motion $H_\mathrm{F} \to H$, one has $Q_E(t) = 0$. In the opposite limit of large Trotter steps, i.e., in the many-body quantum chaotic region, we expect full delocalization over all eigenstates, yielding $Q_E(t) \to 1$ in the long-time limit. Thus, $Q_E(t)$ defines a system-independent measure for the simulation accuracy. From an alternative perspective, $Q_E(t)$ quantifies heating in the effective periodically driven system, as it has been studied previously in the context of energy localization (*19*).

In Fig. 3C, we show numerical data for the long-time average Q_E. Again, we find a sharp threshold between the localized and quantum chaotic regimes. For small Trotter steps, Q_E acquires only a weak quadratic dependence on τ (see Fig. 3D), yielding

$$Q_E \equiv Q_E(t\to\infty) = (\tau/\tau_E)^\alpha, \tau \ll \tau_E \tag{9}$$

with $\alpha = 2$. While τ_E depends on the microscopic details of the system, we find from our numerics that there is no notable dependence on N even in the asymptotic long-time limit, with potential corrections in the thermodynamic limit $N \to \infty$ that are discussed further below.

To obtain an analytical understanding for the observations of weak Trotter errors on local observables, let us start by considering the Magnus expansion for the Floquet Hamiltonian in Eq. 4, which quantifies the leading-order corrections due to time discretization on a Hamiltonian level. From our numerical results for Q_E, we anticipate that the target Hamiltonian H is an almost conserved quantity, which motivates us to study the perturbative corrections to strict energy conservation. Using time-dependent perturbation theory up to second order in the Trotter step size τ, we find

$$Q_E = q_E(h\tau)^2 + \mathcal{O}[(h\tau)^3] \tag{10}$$

The explicit derivation and the final formula for q_E are given in Materials and Methods. For the considered parameters, we estimate $q_E = 0.18$. As it can be seen in Fig. 3D, this analytical value matches well the numerical results.

To test whether the errors on other local observables are also controlled by the emergent constant of motion in the localized regime, we exemplarily study the corrections to the targeted magnetization dynamics. From time-dependent perturbation theory we obtain $\Delta M = m(J\tau)^2 + \mathcal{O}[(J\tau^3)]$ with $m = 0.05$. This theoretical prediction is again very close to the numerical data (see Fig. 3B). As these findings indicate, in the regular region at small Trotter steps, the discretization error on local observables can be captured by time-dependent perturbation theory in the Trotter step size τ—even in the asymptotic long-time limit.

Our observations give a smaller error on local observables than suggested by general considerations on Floquet dynamics in high-frequency regimes (corresponding to small Trotter steps) (*32*, *33*). In these works, it is shown that there exists a static local Hamiltonian $\tilde{H}$, which approximates, with exponentially small error on local observables, the stroboscopic Floquet long-time dynamics in the regimes relevant also for the present case. In the derivation of these results, however, it turns out that this Hamiltonian is $\tilde{H}$, in general, different from H. Our results show that the evolution can be approximated by H itself, as is desired within DQS, while the errors in local observables are now polynomial in τ.

DISCUSSION

As we have shown, intrinsic Trotter errors in DQS are controllable for local observables, with a sharp threshold separating a localized from a many-body quantum chaotic regime. We have achieved this by identifying the Trotterized time evolution on general grounds with an effective time-periodic Floquet problem. As a consequence, the dynamics is constrained by an emergent conserved quantity given by the Floquet Hamiltonian H_F in Eq. 3. While the target Hamiltonian H is not conserved in the Trotterized dynamics, in the localized regime, H remains almost conserved up to perturbative corrections for small Trotter steps τ. This finding does not hold anymore in the many-body quantum chaotic regime, where Trotter errors proliferate and become uncontrollable. While we present data here for a specific model and a specific initial state, our arguments remain general; we find similar properties also for other initial conditions and other model systems such as the recently experimentally realized lattice Schwinger model, which we discuss in the Supplementary Materials. Furthermore, analogous behavior is also found in long-ranged spin models (*34*). Our numerical studies are based on up to $N = 20$ qubits, which is within realized and expected size ranges of digital quantum simulators (*4*–*13*, *35*–*38*).

For experiments, it is of particular interest to assess the precise value of the threshold scale τ^*. Theoretically predicting τ^* is in general as

difficult as solving the desired time evolution. Nevertheless, one can estimate τ^* as follows. Before running an experiment, one can numerically calculate Q_E for small N, yielding a first estimate on τ^*. From this starting point, experiments can find an optimal Trotter step at larger N by decreasing τ until sufficient convergence is reached. Once in the perturbative regime, one can use data at nonzero τ to extrapolate to the ideal dynamics in a well-defined way.

For concrete experimental realizations, it is furthermore of relevance how Trotter errors behave on short to intermediate time scales. From Fig. 1B, one can anticipate that the long-time Trotter error emerges already on rather short time scales. In the Supplementary Materials, we study this transient dynamics in more detail. As we show there for the considered Ising chain, the buildup of the sharp threshold between controllable Trotter errors and quantum chaotic behavior can be observed already on experimentally relevant time scales.

While our results appear to be robust upon increasing the number of degrees of freedom, a quantitative extrapolation to $N \to \infty$ would require the numerical study of larger systems. In this context, recent works have argued that generic periodically driven systems will eventually heat up indefinitely in the thermodynamic limit (*21*–*23*). This might leave a rather pessimistic impression, but, as we explain now, time discretization errors still remain controllable. Even in the worst-case scenario where such an indefinite heating takes place, the energy growth can still be bounded as long as the Hamiltonian has only short-ranged interactions, via $|E(t) - E_0| \leq Ce^{-\tau_0/\tau}t$ for $\tau \ll \tau_0$ (*22*, *23*, *32*, *33*). Here, C denotes a constant of dimension energy squared, and τ_0 denotes a constant of dimension time, both of which are independent of N. Thus, for a given total simulation time t, one can ensure a maximum allowed error Δ on the simulation accuracy by $Q_E(t)$, choosing τ according to $\tau = \tau_0/\log(ct/\Delta)$ with $c = C|E_{T=\infty} - E_0|$. In this worst-case scenario, the Trotter step size to reach a given accuracy therefore acquires at most a logarithmic dependence on t but remains independent of N. This is still an exponential improvement over the global wave function bounds such as given in Eq. 2. In practice, since it is tunable via τ, this extremely slow intrinsic heating can always be adjusted such that the associated heating rate is smaller than that of other error sources, such that Trotter errors become unimportant.

Therefore, the accuracy of DQS experiments on local observables is limited mainly by extrinsic error sources. While these may in the future be eliminated by error correction (*39*, *40*), for relevant system sizes to solve many-body problems, full error correction is still out of reach with currently available resources. In the Supplementary Materials, we discuss in detail two typical extrinsic error sources, timing errors on individual gates and slow drifts of gate couplings over various shots of the experiment. The slow drifts turn out to be relatively benign, leading only to an effective average over an ensemble of target Hamiltonians. Individual timing errors, however, induce in the limit of small τ, a time scale beyond which the accuracy of DQS is severely affected. In addition, a realistic implementation on a physical device will suffer from other potential imperfections, many of which can be very device specific. Typical error sources include qubit decoherence and faulty pulses such as imperfect swaps between internal levels. Both of these make it highly preferable to use as few gates as possible. In view of these, our results become particularly relevant: As they show, intrinsic errors in DQS remain controlled even with relatively large Trotter steps. This makes it possible to reach a desired simulation time with a reduced number of gates, thus diminishing the influence of extrinsic errors and enhancing the accuracy in DQS for local observables.

MATERIALS AND METHODS

Numerical methods and gate sequences

The numerical data shown in this work was obtained for a quantum Ising chain with the Hamiltonian

$$H = H_Z + H_X \tag{11}$$

where

$$H_Z = J\sum_{l=1}^{N-1} S_l^z S_{l+1}^z + h\sum_{l=1}^{N} S_l^z, H_X = g\sum_{l=1}^{N} S_l^x \tag{12}$$

Many of the involved contributions in this model Hamiltonian mutually commute. Therefore, only a small set of elementary quantum gates is required to simulate the Trotterized dynamics. We used the following sequence of two gates

$$U^{(1)} = U_1 U_2, U_1 = e^{-i\tau H_Z}, U_2 = e^{-i\tau H_X} \tag{13}$$

For the presented simulations of observables, we computed the real-time evolution for 2×10^4 periods, except otherwise noted, using a Lanczos algorithm with full reorthogonalization. Because, for a finite-size system, observables still show remaining temporal fluctuations, we extracted the asymptotic long-time limit of the presented quantities by performing a stroboscopic time average over the last 10^4 periods. This large number of Trotter steps is far beyond realistic current-day implementations and serves here only as a worst-case scenario. However, when the Trotter errors on local observables can be controlled even in this idealized limit, one can expect the same to hold true on shorter times relevant for current experiments. In the Supplementary Materials, we illustrate in more detail how the Trotter error builds up on short time scales.

The IPR shown in Fig. 2 can, in principle, be obtained either by exact diagonalization or by use of a dynamical evolution. We chose the latter because it allows us to reach larger systems and is, in principle, an experimentally accessible approach. Dynamically, the IPR can be obtained by a stroboscopic mean

$$\mathrm{IPR} = \lim_{n\to\infty} \frac{1}{n}\sum_{l=1}^{n} \mathcal{P}_l, \mathcal{P}_l = |\langle\psi_0|e^{-ilH_F\tau}|\psi_0\rangle|^2 \tag{14}$$

as one can prove by expanding $\mathcal{P}_l$ in the eigenbasis of H_F, followed by a summation of the resulting geometric series. Note that $\mathcal{P}_l$ is the Loschmidt echo, a common indicator for quantum chaotic behavior in single-particle systems (*27*).

For the computation of the OTO correlator $\mathcal{F}(t)$ defined in Eq. 6, we decompose $\mathcal{F}(n\tau)$ as

$$\mathcal{F}(n\tau) = \langle\psi_1(n\tau)|\psi_2(n\tau)\rangle \tag{15}$$

where the two states

$$|\psi_1(n\tau)\rangle = We^{iH_F n\tau}Ve^{-iH_F n\tau}|\psi_0\rangle \tag{16}$$

$$|\psi_2(n\tau)\rangle = e^{iH_F n\tau} V e^{-iH_F n\tau} W|\psi_0\rangle \tag{17}$$

can be obtained from forward and backward evolving the quantum many-body state with appropriate insertions of the W and V operators. Since the backward evolution has to be performed for every Trotter step n, the overall runtime of this approach scales proportional to n^2. This limits the accessible total simulation time $t = n\tau$. We used $n = 10^3$ for the data shown in Fig. 2B and we performed a stroboscopic average over the last 300 periods to obtain an estimate for the asymptotic long-time value.

Trotter errors on local observables from perturbation theory

As mentioned before, the Trotter errors for local observables can be captured using time-dependent perturbation theory in the limit of sufficiently small τ. In the following, we outline how to obtain the analytical expressions for the coefficients q_E and m for Q_E and $\mathcal{M}$, respectively. First, we consider the simulation accuracy Q_E and, afterward, the Trotter errors on the magnetization $\mathcal{M}$.

For the derivation of the corrections appearing in Q_E, we utilize the energy of the target Hamiltonian H, and therefore, the simulation accuracy Q_E exhibits a substantial overlap with the emergent conserved quantity H_F

$$\langle H_F(n\tau)\rangle_\tau = \langle H_F\rangle = \text{const.} \tag{18}$$

Here, $\langle\mathcal{O}(n\tau)\rangle_\tau = \langle\psi_0|e^{iH_F n\tau}\mathcal{O}e^{-iH_F n\tau}|\psi_0\rangle$ denotes the full Trotterized time evolution with Trotter step size τ as in the main text. Moreover, we define the expectation values in the initial state via $\langle\mathcal{O}\rangle = \langle\psi_0|\mathcal{O}|\psi_0\rangle$ and under the ideal time evolution as $\langle\mathcal{O}(t)\rangle = \langle\mathcal{O}(t)\rangle_{\tau=0}$.

To obtain all corrections to the desired order, we first express H_F using the Magnus expansion up to second order in the Trotter step size

$$H_F = H + \tau C_1 + \tau^2 C_2 + \mathcal{O}(\tau^3) \tag{19}$$

with

$$C_1 = \frac{i}{2}[H_X, H_Z],\ C_2 = -\frac{1}{12}[H_X - H_Z, [H_X, H_Z]] \tag{20}$$

For convenience, we restrict the presentation from now on to a sequence of two elementary gates within one period, as we have for the case of the simulated quantum Ising chain. Using the above expansion for H_F in combination with the conservation of H_F, one obtains for the energy deviation

$$\begin{aligned}\Delta E(n\tau) &= \langle H(n\tau)\rangle_\tau - \langle H\rangle,\\ &= \tau\Delta C_1(n\tau) + \tau^2\Delta C_2(n\tau)\end{aligned} \tag{21}$$

where

$$\Delta C_\nu(n\tau) = \langle C_\nu\rangle - \langle C_\nu(n\tau)\rangle_\tau,\ \nu = 1, 2 \tag{22}$$

As a next step, we use time-dependent perturbation theory to determine the leading order in τ corrections of $\Delta C_\nu(n\tau)$. For this purpose, we write

$$e^{-iH_F t} = e^{-iHt}W(t),\ W(t) = \mathcal{T}e^{-i\int_0^t dt' V(t')} \tag{23}$$

with $\mathcal{T}$ denoting the time-ordering prescription and

$$V(t) = e^{iHt}Ve^{-iHt},\ V = \tau\mathcal{C}_1 + \tau^2\mathcal{C}_2 \tag{24}$$

For the corrections to $\Delta E(n\tau)$ quadratic in τ, we need to perform the time-dependent perturbation theory to first order in τ for $\mathcal{C}_1$ and can neglect any τ-dependent contributions for $\mathcal{C}_2$.

Let us first consider $\Delta\mathcal{C}_1(n\tau)$, which gives

$$\Delta\mathcal{C}_1(n\tau) = \langle\mathcal{C}_1\rangle - \langle\mathcal{C}_1(n\tau)\rangle - i\tau\int_0^{n\tau} dt'\langle[\mathcal{C}_1(t'), \mathcal{C}_1(n\tau)]\rangle \tag{25}$$

The time integral can be conveniently evaluated by recognizing that

$$\mathcal{C}_1 = \frac{i}{2}[H_X, H_Z] = \frac{i}{2}[H, H_Z] \tag{26}$$

since $H = H_X + H_Z$ and thus

$$\mathcal{C}_1(t) = \frac{1}{2}\frac{d}{dt}H_Z(t) \tag{27}$$

This gives

$$\Delta\mathcal{C}_1(n\tau) = \langle\mathcal{C}_1\rangle - \langle\mathcal{C}_1(n\tau)\rangle - \frac{i\tau}{2}\langle[H_Z(n\tau) - H_Z, \mathcal{C}_1(n\tau)]\rangle \tag{28}$$

In the limit of $n \to \infty$, we can use the general property that expectation values of operators are governed by the so-called diagonal ensemble (*31*)

$$\langle\mathcal{O}(n\tau)\rangle \xrightarrow{n\to\infty} \sum_\lambda p_\lambda\langle\lambda|\mathcal{O}|\lambda\rangle \tag{29}$$

where $p_\lambda = |\langle\lambda|\psi_0\rangle|^2$ and the set of all $|\lambda\rangle$ denotes the eigenstates for the target Hamiltonian H. Using particular properties of the considered protocol, the above result for $\Delta\mathcal{C}_1(n\tau)$ can be simplified considerably. We can use, for example, that $\langle\mathcal{C}_1\rangle = 0$ and $\langle[H_Z, \mathcal{C}_1(n\tau)]\rangle = 0$, because $|\psi_0\rangle$ is an eigenstate for H_Z, which lastly yields

$$\Delta\mathcal{C}_1(n\tau) \xrightarrow{n\to\infty} -\frac{\tau}{4}\sum_\lambda p_\lambda\langle\lambda|[H_Z, [H_Z, H_X]]|\lambda\rangle \tag{30}$$

For the contributions to $\Delta E(n\tau)$ that are second order in τ stemming from $\Delta\mathcal{C}_2(n\tau)$, we can restrict to the zeroth order in time-dependent perturbation theory for $\langle\mathcal{C}_2(n\tau)\rangle_\tau$, i.e., we can replace $\langle\mathcal{C}_2(n\tau)\rangle_\tau \to \langle\mathcal{C}_2(n\tau)\rangle$. This yields

$$\Delta\mathcal{C}_2(n\tau) \xrightarrow{n\to\infty} \langle\mathcal{C}_2\rangle - \sum_\lambda p_\lambda\langle\lambda|\mathcal{C}_2|\lambda\rangle \tag{31}$$

Collecting all contributions, we lastly obtain

$$Q_E = \frac{\Delta E}{E_{T=\infty} - E_0} = q_E (h\tau)^2 + \mathcal{O}[(h\tau)^3] \tag{32}$$

with

$$q_E = \frac{1}{J^2 E_0}\left[\langle \mathcal{C}_2\rangle - \sum_\lambda p_\lambda \langle\lambda|\mathcal{C}_2|\lambda\rangle - -\frac{1}{4}\sum_\lambda p_\lambda \langle\lambda|[H_Z,[H_Z,H_X]]|\lambda\rangle\right] \tag{33}$$

given that $E_{T=\infty} = 0$. This expression can be evaluated using full diagonalization, which provides access to all eigenstates $|\lambda\rangle$. For the considered parameters of our simulations, we find $q_E = 0.18$, which is consistent with the full dynamical calculation in the small Trotter step limit (see Fig. 3D).

For estimating the lowest-order corrections in τ for other observables such as the magnetization $\mathcal{M}$, we can not make direct use of the emergent conserved quantity H_F as for the energy of the target Hamiltonian. Still, we can perform time-dependent perturbation theory, which we now have to carry out up to second order. Following the same steps as before, we obtain the following expression for the magnetization

$$\begin{aligned}\Delta\mathcal{M}(n\tau) &= \langle \mathcal{M}(n\tau)\rangle_\tau - \langle \mathcal{M}(n\tau)\rangle = \\ &= \frac{\tau^2}{12}\left[\langle\{H_Z^2(n\tau), \mathcal{M}(n\tau)\}\rangle - E_Z^2\langle\mathcal{M}(t)\rangle\right] \\ &\quad + i\frac{\tau^2}{6}\langle[\mathcal{C}_1(n\tau) - \mathcal{C}_1, \mathcal{M}(n\tau)]\rangle \\ &\quad - \frac{5\tau^2}{12}\int_0^{n\tau} dt\langle \mathcal{C}_1(t) H_Z(t) M(n\tau) + \text{h.c.}\rangle \end{aligned} \tag{34}$$

Here, $\{A, B\} = AB + BA$ denotes the anticommutator, and E_Z is given by $H_Z|\psi_0\rangle = E_Z|\psi_0\rangle$. In the limit $n \to \infty$, we can again use that expectation values can be evaluated in the diagonal ensemble. In addition, the expression involving the time integral can be formally solved using the Lehman representation. Last, we obtain

$$\Delta\mathcal{M}(n\tau) \xrightarrow{n\to\infty} m(h\tau)^2 + \mathcal{O}[(h\tau)^3] \tag{35}$$

with

$$\begin{aligned} m = &\frac{1}{12J^2}\sum_\lambda p_\lambda \langle\lambda|\{H_Z^2, \mathcal{M}\} - E_Z^2\mathcal{M}|\lambda\rangle \\ &- \frac{1}{6J^2}\sum_\lambda p_\lambda \text{Re}[\langle\lambda|[H_X, M]H_Z|\lambda\rangle] \\ &+ \frac{1}{6J^2}\sum_{\lambda,\lambda'}\frac{p_\lambda}{E_\lambda - E_{\lambda'}}\text{Re}[\langle\lambda|[H_Z, H_X]H_Z|\lambda'\rangle\langle\lambda'|\mathcal{M}|\lambda\rangle] \\ &+ \frac{1}{6J^2}\sum_{\lambda,\lambda'}\frac{\langle\lambda|\mathcal{M}|\lambda\rangle}{E_\lambda - E_{\lambda'}}\text{Re}[C_\lambda C_{\lambda'}^*\langle\lambda|[H_Z, H_X]H_Z|\lambda'\rangle] \end{aligned} \tag{36}$$

where $C_\lambda = \langle\lambda|\psi_0\rangle$ and E_λ denotes the eigenenergies of the target Hamiltonian H corresponding to the eigenstate $|\lambda\rangle$. Using full diagonalization, we can again evaluate this expression yielding for our model a value of $m = 0.05$, which we used in Fig. 3B for the asymptotic small τ prediction and which matches well the result from the full dynamics. Notice that for the presented derivation of the perturbative corrections for the magnetization $\mathcal{M}$, we used explicitly that the initial state is an eigenstate of $\mathcal{M}$. Choosing different observables or different initial conditions might yield linearly in τ contributions as the leading-order corrections.

SUPPLEMENTARY MATERIALS

Supplementary material for this article is available at http://advances.sciencemag.org/cgi/content/full/5/4/eaau8342/DC1

Section S1. Temporal buildup of the Trotter error threshold
Section S2. Trotter errors in the Ising model for alternative initial condition
Section S3. Trotter errors in the lattice Schwinger model
Section S4. Imperfections
Fig. S1. Temporal buildup of Trotter errors on transient time scales.
Fig. S2. Simulation accuracy Q_E for initial Neel state.
Fig. S3. IPR for the DQS of the lattice Schwinger model.
Fig. S4. Trotter errors for the DQS of the lattice Schwinger model.
Fig. S5. Timing errors in the dynamics of the simulation accuracy $Q_E(t)$ for the Ising model.
Reference (*41*)

REFERENCES AND NOTES

1. T. D. Ladd, F. Jelezko, R. Laflamme, Y. Nakamura, C. Monroe, J. L. O'Brien, Quantum computers. *Nature* **464**, 45–53 (2010).
2. R. P. Feynman, Simulating physics with computers. *Int. J. Theor. Phys.* **21**, 467–488 (1982).
3. S. Lloyd, Universal quantum simulators. *Science* **273**, 1073–1078 (1996).
4. P. J. J. O'Malley, R. Babbush, I. D. Kivlichan, J. Romero, J. R. McClean, R. Barends, J. Kelly, P. Roushan, A. Tranter, N. Ding, B. Campbell, Y. Chen, Z. Chen, B. Chiaro, A. Dunsworth, A. G. Fowler, E. Jeffrey, E. Lucero, A. Megrant, J. Y. Mutus, M. Neeley, C. Neill, C. Quintana, D. Sank, A. Vainsencher, J. Wenner, T. C. White, P. V. Coveney, P. J. Love, H. Neven, A. Aspuru-Guzik, J. M. Martinis, Scalable quantum simulation of molecular energies. *Phys. Rev. X* **6**, 031007 (2016).
5. A. Kandala, A. Mezzacapo, K. Temme, M. Takita, M. Brink, J. M. Chow, J. M. Gambetta, Hardware-efficient variational quantum eigensolver for small molecules and quantum magnets. *Nature* **549**, 242–246 (2017).
6. C. Hempel, C. Maier, J. Romero, J. McClean, T. Monz, H. Shen, P. Jurcevic, B. Lanyon, P. Love, R. Babbush, A. Aspuru-Guzik, R. Blatt, C. Roos, Quantum chemistry calculations on a trapped-ion quantum simulator. *Phys. Rev. X* **8**, 031022 (2018).
7. B. P. Lanyon, C. Hempel, D. Nigg, M. Müller, R. Gerritsma, F. Zähringer, P. Schindler, J. T. Barreiro, M. Rambach, G. Kirchmair, M. Hennrich, P. Zoller, R. Blatt, C. F. Roos, Universal digital quantum simulation with trapped ions. *Science* **334**, 57–61 (2011).
8. Y. Salathé, M. Mondal, M. Oppliger, J. Heinsoo, P. Kurpiers, A. Potočnik, A. Mezzacapo, U. Las Heras, L. Lamata, E. Solano, S. Filipp, A. Wallraff, Digital quantum simulation of spin models with circuit quantum electrodynamics. *Phys. Rev. X* **5**, 021027 (2015).
9. J. Barreiro, M. Müller, P. Schindler, D. Nigg, T. Monz, M. Chwalla, M. Hennrich, C. F. Roos, P. Zoller, R. Blatt, An open-system quantum simulator with trapped ions. *Nature* **470**, 486–491 (2011).
10. R. Barends, L. Lamata, J. Kelly, L. García-Álvarez, A. G. Fowler, A. Megrant, E. Jeffrey, T. C. White, D. Sank, J. Y. Mutus, B. Campbell, Y. Chen, Z. Chen, B. Chiaro, A. Dunsworth, I.-C. Hoi, C. Neill, P. J. J. O'Malley, C. Quintana, P. Roushan, A. Vainsencher, J. Wenner, E. Solano, J. M. Martinis, Digital quantum simulation of fermionic models with a superconducting circuit. *Nat. Commun.* **6**, 7654 (2015).
11. N. K. Langford, R. Sagastizabal, M. Kounalakis, C. Dickel, A. Bruno, F. Luthi, D. J. Thoen, A. Endo, L. DiCarlo, Experimentally simulating the dynamics of quantum light and matter at deep-strong coupling. *Nat. Commun.* **8**, 1715 (2017).
12. K. X. Wei, C. Ramanathan, P. Cappellaro, Exploring localization in nuclear spin chains. *Phys. Rev. Lett.* **120**, 070501 (2018).
13. E. A. Martinez, C. A. Muschik, P. Schindler, D. Nigg, A. Erhard, M. Heyl, P. Hauke, M. Dalmonte, T. Monz, P. Zoller, R. Blatt, Real-time dynamics of lattice gauge theories with a few-qubit quantum computer. *Nature* **534**, 516–519 (2016).
14. D. W. Berry, G. Ahokas, R. Cleve, B. C. Sanders, Efficient quantum algorithms for simulating sparse hamiltonians. *Commun. Math. Phys.* **270**, 359–371 (2007).

15. D. Poulin, M. B. Hastings, D. Wecker, N. Wiebe, A. C. Doherty, M. Troyer, The Trotter step size required for accurate quantum simulation of quantum chemistry. *Quantum Inf. Comput.* **15**, 361–384 (2015).
16. R. Babbush, J. McClean, D. Wecker, A. Aspuru-Guzik, N. Wiebe, Chemical basis of Trotter-Suzuki errors in quantum chemistry simulation. *Phys. Rev. A* **91**, 022311 (2015).
17. P. W. Anderson, Absence of diffusion in certain random lattices. *Phys. Rev.* **109**, 1492–1505 (1958).
18. D. M. Basko, I. L. Aleiner, B. L. Altshuler, Metal–insulator transition in a weakly interacting many-electron system with localized single-particle states. *Ann. Phys.* **321**, 1126–1205 (2006).
19. L. D'Alessio, A. Polkovnikov, Many-body energy localization transition in periodically driven systems. *Ann. Phys.* **333**, 19–33 (2013).
20. S. Blanes, F. Casas, J. A. Oteo, J. Ros, The Magnus expansion and some of its applications. *Phys. Rep.* **470**, 151–238 (2009).
21. A. Lazarides, A. Das, R. Moessner, Equilibrium states of generic quantum systems subject to periodic driving. *Phys. Rev. E* **90**, 012110 (2014).
22. D. A. Abanin, W. D. Roeck, F. Huveneers, Exponentially slow heating in periodically driven many-body systems. *Phys. Rev. Lett.* **115**, 256803 (2015).
23. T. Mori, T. Kuwahara, K. Saito, Rigorous bound on energy absorption and generic relaxation in periodically driven quantum systems. *Phys. Rev. Lett.* **116**, 120401 (2016).
24. X. Peng, J. Du, D. Suter, Quantum phase transition of ground-state entanglement in a Heisenberg spin chain simulated in an NMR quantum computer. *Phys. Rev. A* **71**, 012307 (2005).
25. R. Barends, A. Shabani, L. Lamata, J. Kelly, A. Mezzacapo, U. Las Heras, R. Babbush, A. G. Fowler, B. Campbell, Y. Chen, Z. Chen, B. Chiaro, A. Dunsworth, E. Jeffrey, E. Lucero, A. Megrant, J. Y. Mutus, M. Neeley, C. Neill, P. J. J. O'Malley, C. Quintana, P. Roushan, D. Sank, A. Vainsencher, J. Wenner, T. C. White, E. Solano, H. Neven, J. M. Martinis, Digitized adiabatic quantum computing with a superconducting circuit. *Nature* **534**, 222–226 (2016).
26. P. Jurcevic, H. Shen, P. Hauke, C. Maier, T. Brydges, C. Hempel, B. P. Lanyon, M. Heyl, R. Blatt, C. F. Roos, Direct observation of dynamical quantum phase transitions in an interacting many-body system. *Phys. Rev. Lett.* **119**, 080501 (2017).
27. F. Haake, *Quantum Signatures of Chaos* (Springer, 2010).
28. N. Ullah, C. E. Porter, Expectation value fluctuations in the unitary ensemble. *Phys. Rev.* **132**, 948–950 (1963).
29. J. Maldacena, S. H. Shenker, D. Stanford, A bound on chaos. *J. High Energy Phys.* **2016**, 106 (2016).
30. I. Kukuljan, S. Grozdanov, T. Prosen, Weak quantum chaos. *Phys. Rev. B* **96**, 060301 (2017).
31. L. D'Alessio, Y. Kafri, A. Polkovnikov, M. Rigol, From quantum chaos and eigenstate thermalization to statistical mechanics and thermodynamics. *Adv. Phys.* **65**, 239–362 (2016).
32. T. Kuwahara, T. Mori, K. Saito, Floquet–Magnus theory and generic transient dynamics in periodically driven many-body quantum systems. *Ann. Phys.* **367**, 96–124 (2016).
33. D. A. Abanin, W. De Roeck, W. W. Ho, F. Huveneers, Effective Hamiltonians, prethermalization, and slow energy absorption in periodically driven many-body systems. *Phys. Rev. B* **95**, 014112 (2017).
34. L. M. Sieberer, T. Olsacher, A. Elben, M. Heyl, P. Hauke, F. Haake, P. Zoller, Digital Quantum Simulation, Trotter Errors, and Quantum Chaos of the Kicked Top. arXiv:1812.05876 [quant-ph] (14 December 2018).
35. H. Bernien, S. Schwartz, A. Keesling, H. Levine, A. Omran, H. Pichler, S. Choi, A. S. Zibrov, M. Endres, M. Greiner, V. Vuletić, M. D. Lukin, Probing many-body dynamics on a 51-atom quantum simulator. *Nature* **551**, 579–584 (2017).
36. J. Zhang, G. Pagano, P. W. Hess, A. Kyprianidis, P. Becker, H. Kaplan, A. V. Gorshkov, Z.-X. Gong, C. Monroe, Observation of a many-body dynamical phase transition with a 53-qubit quantum simulator. *Nature* **551**, 601–604 (2017).
37. J. S. Otterbach, R. Manenti, N. Alidoust, A. Bestwick, M. Block, B. Bloom, S. Caldwell, N. Didier, E. Schuyler Fried, S. Hong, P. Karalekas, C. B. Osborn, A. Papageorge, E. C. Peterson, G. Prawiroatmodjo, N. Rubin, C. A. Ryan, D. Scarabelli, M. Scheer, E. A. Sete, P. Sivarajah, R. S. Smith, A. Staley, N. Tezak, W. J. Zeng, A. Hudson, B. R. Johnson, M. Reagor, M. P. da Silva, C. Rigetti, Unsupervised Machine Learning on a Hybrid Quantum Computer. arXiv:1712.05771 [quant-ph] (15 December 2017).
38. C. Neill, P. Roushan, K. Kechedzhi, S. Boixo, S. V. Isakov, V. Smelyanskiy, A. Megrant, B. Chiaro, A. Dunsworth, K. Arya, R. Barends, B. Burkett, Y. Chen, Z. Chen, A. Fowler, B. Foxen, M. Giustina, R. Graff, E. Jeffrey, T. Huang, J. Kelly, P. Klimov, E. Lucero, J. Mutus, M. Neeley, C. Quintana, D. Sank, A. Vainsencher, J. Wenner, T. C. White, H. Neven, J. M. Martinis, A blueprint for demonstrating quantum supremacy with superconducting qubits. *Science* **360**, 195–199 (2018).
39. P. Schindler, J. T. Barreiro, T. Monz, V. Nebendahl, D. Nigg, M. Chwalla, M. Hennrich, R. Blatt, Experimental repetitive quantum error correction. *Science* **332**, 1059–1061 (2011).
40. M. D. Reed, L. DiCarlo, S. E. Nigg, L. Sun, L. Frunzio, S. M. Girvin, R. J. Schoelkopf, Realization of three-qubit quantum error correction with superconducting circuits. *Nature* **482**, 382–385 (2012).
41. C. W. Gardiner, P. Zoller, *Quantum Noise* (Springer, 2000).

Acknowledgments: We thank A. Polkovnikov for invaluable discussions in the initial stages of this work as well as L. Sieberer, A. Elben, and T. Olsacher for various comments and suggestions on the manuscript. **Funding:** Work at Innsbruck was supported by ERC Synergy grant UQUAM and the SFB FoQuS (FWF project no. F4016-N23). M.H. acknowledges support by the Deutsche Forschungsgemeinschaft (DFG) via the Gottfried Wilhelm Leibniz Prize program. P.H. acknowledges support by the DFG Collaborative Research Centre SFB 1225 (ISOQUANT) and the ERC Advanced Grant EntangleGen (project ID 694561). **Author contributions:** P.Z. proposed the research. P.H. and M.H. performed the analytical calculations and analyzed the data. M.H. performed the numerical simulations. All authors discussed the results and wrote the manuscript. **Competing interests:** The authors declare that they have no competing interests. **Data and materials availability:** All data needed to evaluate the conclusions in the paper are present in the paper and/or the Supplementary Materials. Additional data available from the first author upon request.

Submitted 19 July 2018
Accepted 14 February 2019
Published 12 April 2019
10.1126/sciadv.aau8342

Citation: M. Heyl, P. Hauke, P. Zoller, Quantum localization bounds Trotter errors in digital quantum simulation. *Sci. Adv.* **5**, eaau8342 (2019).

Science Advances

Quantum localization bounds Trotter errors in digital quantum simulation

Markus Heyl, Philipp Hauke and Peter Zoller

Sci Adv **5** (4), eaau8342.
DOI: 10.1126/sciadv.aau8342